RESEARCH

Palladium Nanoparticles Anchored on Magnetic Organic–Inorganic Hybrid 3D-Network Polymer: A Nanocatalyst for Reduction of Nitro Compounds and Suzuki–Miyaura Coupling

Setareh Moradi[1] · Roya Mozafari[1] · Mohammad Ghadermazi[1]

Abstract

$CoFe_2O_4$@3D-Network polymers-K22.Pd was synthesized by grafting Kryptofix-22 moieties onto the surface of magnetic 3D-network polymers, followed by a reaction of the nanocomposite with Palladium (II) nitrate. The cavities of the Kryptofix-22 host material can effectively stabilize the Pd nanoparticles and prevent their aggregation and separation from the surface. Using advanced characterization techniques, such as FT-IR, BET, TGA, FE-SEM, TEM, XRD, EDX, and VSM, thorough understanding of the catalyst structure and morphology was facilitated and confirmed, its expected properties. The catalyst has been efficiently applied to Suzuki reactions and reduction of nitro compound derivatives. Its primary advantages include mild reaction conditions, high efficiency, and shorter reaction times than traditional methods. One of the greatest benefits of this catalyst is its reusability. It can be easily separated from the reaction mixture using a magnetic force and reused for up to five cycles without significant activity loss. This is important for sustainable chemistry, as it reduces waste and potentially lowers costs.

Keywords 3D-network porous polymer · Nanocomposite · Palladium (II) nitrate · Kryptofix-22 · Suzuki reactions · Amine reduction

1 Introduction

The development of magnetic nanoparticles embedded in polymeric networks, leading to the synthesis of novel nanocomposites has been a central area of research in recent years. This is especially true in the academic and pharmaceutical industries, where such technology can be applied in drug delivery systems, targeted therapies, magnetic resonance imaging, and other applications [1–3].

On the other hand, solid-support heterogeneous metal catalysts offer numerous benefits compared to their homogeneous counterparts. From both economic and environmental perspectives, their easy preparation, product purification, low cost, convenient reaction handling, and simple catalyst recyclability make them an appealing choice. The ability to heterogenize catalysts onto solid supports can effectively reduce catalyst waste, offering a sustainable approach to many chemical processes [4–6].

Porous organic polymers (POPs) are indeed a significant class of functional materials. Their key characteristics, such as suitable pore distribution size, large surface area, ease of synthesis, non-toxicity, and low cost make them highly applicable in various fields such as chemical catalysts and nanotechnology [7, 8].

Furthermore, functionalized POPs can increase the diffusion properties due to enhanced porosity, which results in greater accessibility to active sites, thereby improving the catalytic performance [9–12].

3D-network polymers based on calix[4]resorcinarene have gained significant attention in surface modification due to their unique branched structure. The large number of terminal groups in their structure allows easy modification with target molecules through covalent linkages, thereby enhancing the functionality of these polymers. Calixarenes and calixresorcinarenes are promising candidates for developing solid-support porous organic polymers. Their synthesis process is straightforward, and they possess distinct properties such as high thermal and chemical stability [13–17].

✉ Mohammad Ghadermazi
mghadermazi@yahoo.com

1 Department of Chemistry, Faculty of Science, University of Kurdistan, Sanandaj, Iran

Kryptofix-22, a type of aza-crown ether, is renowned for its high affinity and selectivity in binding transition metals. The macrocyclic nature of this compound enables it to encapsulate and surround various metal ions with its oxygen and nitrogen atoms, forming organometallic complexes [18, 19]. The distinctive structure and properties of Kryptofix-22 have led to its widespread use across numerous fields. Its applications span from supramolecular chemistry and materials science to biochemistry, separation techniques, catalysis, and biomedicine. Its ability to form stable complexes with various ions makes it especially valuable in these areas [20–22].

Palladium nanoparticles have been recognized for their high catalytic activity, but their small size poses a significant challenge in terms of separation and recovery, as they cannot be efficiently separated using conventional methods such as centrifugation or filtration [23, 24]. To overcome these challenges, Pd nanoparticles are often loaded into the pores of solid supports or deposited on the surfaces of materials like cellulose, zeolites, polymers, or silica. This approach not only facilitates the recovery and reuse of the catalyst but also often enhances their stability and performance by providing a protective environment [25–28].

The Suzuki–Miyaura cross-coupling reaction is one of the most powerful and widely used methods for forming carbon–carbon (C–C) bonds in modern organic synthesis. The reaction typically involves the cross-coupling of an aryl or vinyl halide with an organoboron compound, facilitated by a palladium catalyst and a base. This reaction operates under relatively mild conditions and generally exhibits high tolerance towards various functional groups, which makes it a remarkably versatile tool for complex molecular construction. The Suzuki–Miyaura reaction has found broad application in numerous fields, including the synthesis of pharmaceuticals, agrochemicals, and materials science [29–31].

Sodium borohydride ($NaBH_4$) is a potent reducing agent often used in organic chemistry. Its ability to reduce nitro groups, which are difficult to reduce under mild conditions, can be significantly enhanced when used in conjunction with metal complexes. This is because these complexes can often activate the nitro group, or synergistically interact with $NaBH_4$ to increase its reducing strength. This makes it possible to selectively reduce nitro groups in the presence of other functional groups that might be more easily reduced, enabling more complex and targeted synthetic pathways [32–35].

Using a calix[4]resorcinarene-based 3D network porous polymer as a heterogeneous catalyst could present several benefits. Firstly, such polymers can be advantageous because they generally offer high surface areas and porosities, which can lead to increased catalyst exposure and improved catalytic activity. Secondly, the use of a calix[4]resorcinarene moiety could provide unique chemical environments due to its conformational flexibility and the ability to form inclusion complexes, which could enhance the catalyst's selectivity. Thirdly, the use of a heterogeneous catalyst would simplify the separation and recovery processes, reducing the environmental impact and improving the overall efficiency of the reaction. Lastly, this kind of catalyst could potentially operate under milder reaction conditions, resulting in less hazardous waste and lower energy consumption, further enhancing its environmental credentials [36, 37]. Thus, the development of such a catalyst could lead to more sustainable and efficient processes for Suzuki reactions and the reduction of nitro compounds.

2 Experimental

2.1 Materials and Instrumentation

All the chemicals and solvents used for the synthesis of $CoFe_2O_4$@3D-Network polymers-K22.Pd, including $FeCl_3 \cdot 6H_2O$, $CoCl_2.6H_2O$, resorcinol, and other chemicals were purchased from Sigma-Aldrich and Merck.

The instruments used for the characterization of $CoFe_2O_4$@3D-Network polymers-K22.Pd included FT-IR, XRD, FE-SEM, TEM, TGA, BET and VSM techniques.

The surface morphology and diameter of the nanocatalyst were studied by SEM-TESCAN MIRA3. The X-ray diffraction (XRD) pattern measurements of the samples and Fourier Transform Infrared (FTIR) spectra were recorded using a Jeol JEM-1010 electron microscope and JEOL JSM-6100 microscope with (Cu kα radiation, $\lambda = 1.54$ Å) in the region of $2\Theta = 20°$- 80° and Perkin Elmer Spectrum one instruments, using potassium bromide discs, respectively. Thermo gravimetric analysis was measured on a TGA instrument of BAHR Thermo analyse STA 503 with the maximum heating rate of 10 °C/min. X-ray spectroscopy (EDX) by a Kevex, Delta Class I, and Shimadzu DTG-60 instrument respectively. Vibrating sample magnetometer (VSM) measurement was recorded by a Vibrating Sample Magnetometer MDKFD. The purity determination of the products and the reaction monitoring were accomplished by TLC on silica gel polygram SILG/UV 254 plates. Additionally, the catalyst's transmission electron microscope (TEM) images were obtained using a Zeiss-EM10C field emission microscope at an accelerating voltage of 200 kV. The surface properties of the samples were determined by nitrogen adsorption/desorption isotherms at − 197 °C using a micromeritics ASAP 2000 instrument and the surface area and the pore size distribution were investigated by the Brunauer–Emmett–Teller (BET) and Barrett–Joyner–Halenda (BJH) analysis.

2.2 Preparation of Calix[4]resorcinarene

Calix[4]resorcinarene was made based on the mentioned procedure [38]. In summary, a solution of 75 mL distilled water and 75 mL HCl (37%) was added to a solution of 16.5 g resorcinol and 75 mL ethanol (95%) in a flask 250 mL, under an N_2 atmosphere at room temperature.

0.15 mol of acetaldehyde was added dropwise to the reaction mixture, the resulting solution was allowed to slowly warm up to 50 °C for 1h. After about 1h, the clear solution turned cloudy and a precipitate separated over time. The reaction mixture was then cooled to ambient temperature and stirred under argon gas for 4 days to complete the reaction. Eventually, the product was filtered, and the obtained precipitates were washed with distilled water for further purification and dried at 60 °C for 10 h.

2.3 Preparation of the Porous Organic Polymer Based on Calix[4]resorcinarene

To synthesize the desired polymeric network, in a 250 mL 3-necked, round-bottomed flask, 0.42 mol of formaldehyde was added to 7.6 g of the prepared calix[4]resorcinarene by dissolving in 40 mL NaOH solution (10%) at room temperature. The mixture was stirred at 90 °C for 20 h. Eventually, the resulting gel was washed several times with cold distilled water and stirred in 50 mL of HCl solution (0.1 M) for 1 h. The solid product was dried at 100 °C for 10 h.

2.4 Synthesis of CoFe$_2$O$_4$@3D-Network Polymers

First, in a 250 mL round bottom flask, 0.5 g of poly calix[4] resorcinarene was ultrasonicated for 30 min in 25 mL distilled water. To the magnetically stirred mixture of as-prepared dispersed poly calix[4]resorcinarene, a solution of 0.0516 g of CoCl$_2$·6H$_2$O and 0.216 g FeCl$_3$·6H$_2$O, in 15 mL distilled water was added to the suspension of poly calix[4] resorcinarene. The mixture was stirred at 80 °C for 45 min. After that, a solution of NaOH (0.1 M) was added dropwise to the reaction solution under constant stirring by a magnetic stirrer until the stabilization of pH to 11. Eventually, the product was separated using a magnet, taking advantage of the magnetic properties of CoFe$_2$O$_4$. Then, the obtained product was washed with distilled water and dried at 70 °C for 12 h.

2.5 Synthesis of CoFe$_2$O$_4$@3D-Network Polymers-K22

In this step, 0.5 g of magnetic polymer was ultrasonicated for 15 min in 100 mL toluene. Then 3 mL of the 3-(Chloropropyl)-trimethoxysilane (CPTES) was added to the flask under N_2 atmosphere at room temperature, and

the mixture was well stirred for 24 h at 70 °C. Ultimately, CoFe$_2$O$_4$@3D-Network polymers-CPTES were collected using an external magnet, washed with ethanol and distilled water, and then dried at 60 °C. During this process, 0.15 g of CoFe$_2$O$_4$@3D-Network polymers-CPTES was first homogenized with 20 mL of dry DMF in an ultrasonic bath for 45 min. Then a few drops of triethylamine (Et$_3$N), and 0.26 g Kryptofix-22 were added to the product and the reaction mixture was sonicated for another 20 min and was stirred for 12 h at 90 °C. The resulting CoFe$_2$O$_4$@3D-Network polymers-K22 was washed with distilled water and then dried at 65 °C.

2.6 Synthesis of Pd Nanoparticles Incorporated to Mesoporous Magnetite Polymer (CoFe$_2$O$_4$@3D-Network Polymers-K22.Pd)

In the final stage, 0.5 g of the above mixture was sonicated in 100 mL of distilled water for 20 min. A solution 0.05 g of Palladium (II) nitrate in 20 mL of distilled water was added to the suspension of CoFe$_2$O$_4$@3D-Network polymers-K22 and the combined solution was refluxed for 24 h, allowing the Palladium (II) nitrate to react with the CoFe$_2$O$_4$@3D-Network polymers-K22. After this reaction time, the resultant product was isolated using an external magnet. Finally, the obtained product was washed with distilled water and dried at 60 °C for 10 h.

2.7 A General Procedure for Reduction of Nitro Compounds with NaBH$_4$ in the Presence of CoFe$_2$O$_4$@3D-Network Polymers-K22.Pd Nanocatalyst

In a round-bottomed flask equipped with a magnetic stirrer, a mixture of 0.03 g CoFe$_2$O$_4$@3D-Network polymers-K22. Pd in 4 mL of distilled water and 1 mmol NaBH$_4$ was provided. After 3 min of stirring, 1 mmol of nitro compound was added to the flask, and the solution was stirred vigorously at room temperature. The progress of the reaction was monitored by TLC. Once the reaction was completed, the magnetic nanocatalyst was easily separated from the reaction mixture using an external magnet. The reduced product was then extracted from the remaining liquid using diethyl ether.

2.8 A General Procedure for Suzuki–Miyaura Coupling Reaction in the Presence of CoFe$_2$O$_4$@3D-Network Polymers-K22.Pd Nanocatalyst

We prepared a round bottom flask, equipped with a magnetic stirrer. Into this flask, we added a mixture of 1 mmol aryl halide, 1 mmol phenylboronic acid, 1.5 mmol potassium
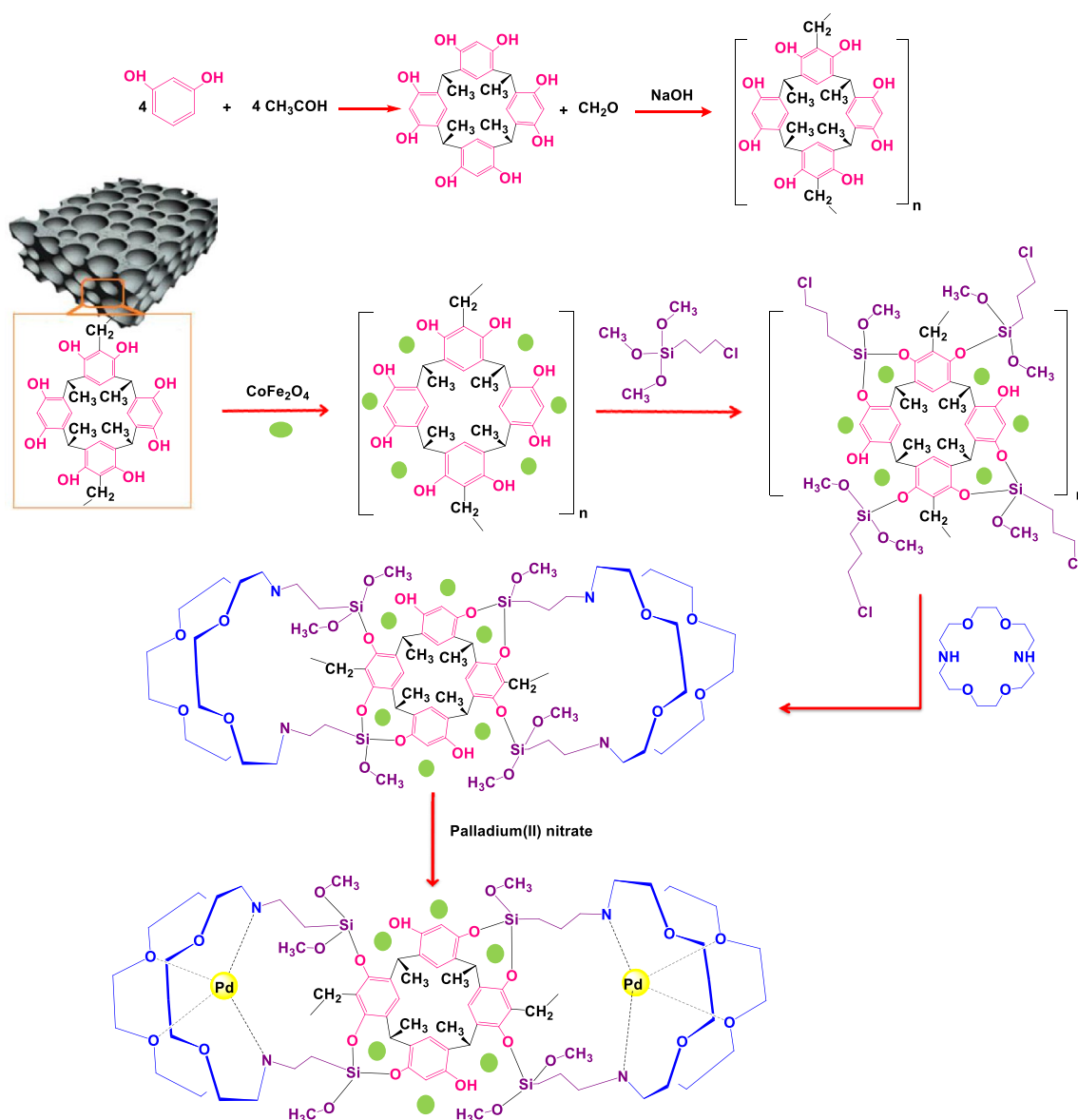
Scheme 1 Synthesis CoFe$_2$O$_4$@3D-Network polymers-K22.Pd catalyst

carbonate (K$_2$CO$_3$), and 0.03 g of CoFe$_2$O$_4$@3D-Network polymers-K22.Pd in 3 mL of distilled water mixture was stirred vigorously at room temperature. The progress of the reaction was monitored by TLC. Once the reaction was complete, the magnetic nanocatalyst was easily separated from the reaction mixture using an external magnet and then washed several times with distilled water. Finally, the pure products of the Suzuki–Miyaura coupling reaction were obtained in high yields.

3 Results and Discussion

3.1 Characterization of CoFe$_2$O$_4$@3D-Network Polymers-K22.Pd Nanocatalyst

The synthetic strategy for the preparation of the CoFe$_2$O$_4$@3D-Network polymers-K22.Pd is summarized in Scheme 1.

The 3D-network porous polymer was prepared through a multi-step process. The process begins with the reaction of resorcinol and acetaldehyde. The polycondensation of calix[4]resorcinarene with formaldehyde is then carried out, resulting in a 3D-network of porous polymer. Next, CoFe$_2$O$_4$ magnetic nanoparticles were deposited onto the

surface of this polymer. This is accomplished through the coprecipitation of Fe^{3+} and Co^{2+} ions in an alkaline solution with pH = 11 to ensure complete precipitation and to control the size and shape of the $CoFe_2O_4$ particles. CPTES reacts with $CoFe_2O_4$@3D-Network polymer, adding a propyl chain with a chlorine atom on the end to functionalize the polymeric network. The Kryptofix-22 reacts with the chlorine on the propyl chain, replacing it and produce $CoFe_2O_4$@3D-Network polymers-K22. Finally, the treatment of this functionalized polymer with Palladium (II) nitrate results in the formation of $CoFe_2O_4$@3D-Network polymers-K22.Pd. This step involves a stable interaction between the Palladium and the functional groups of Kryptofix-22. To confirm the successful synthesis and characterization the nanocatalyst, a series of analytical techniques were employed.

3.1.1 FT-IR Studies

As shown in Fig. 1, FT-IR techniques can characterize and confirm the catalyst's preparation. In the comparative FT-IR spectra of 3D-Network polymers, $CoFe_2O_4$@3D-Network polymers, $CoFe_2O_4$@3D-Network polymers-K22, and $CoFe_2O_4$@3D-Network polymers-K22.Pd, broad bands at the 3100–3600 cm^{-1} range represent the hydroxyl functional group (O–H), and peaks appearing at the 2800–2900 cm^{-1} region are attributed
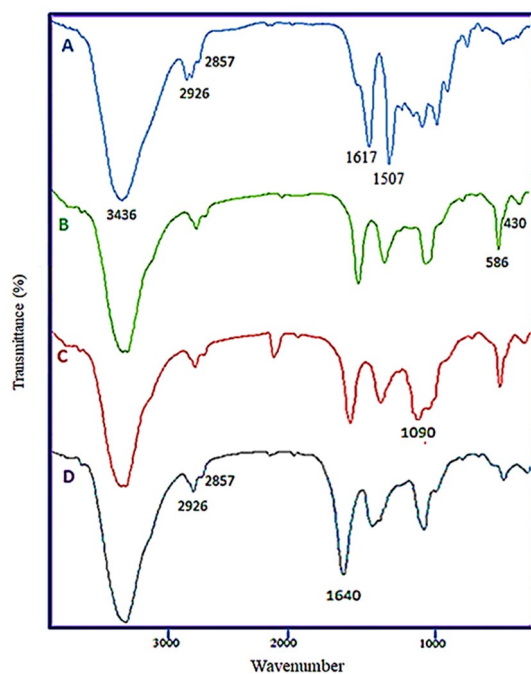
to the stretching vibrations of the C-H group. Peaks at 1507 and 1617 cm^{-1} indicate the presence of phenyl rings in all structures (Fig. 1A) [39]. The peaks at 430 cm^{-1} and 586 cm^{-1} represent the stretching vibrations of Fe–O bonds in the tetrahedral and octahedral sites of $CoFe_2O_4$, respectively (Fig. 1B) [40]. In $CoFe_2O_4$@3D-Network polymers-K22.Pd, a broad peak emerges at 1090 cm^{-1}, indicating the stretching mode of Si–OH in silica [41]. A new broadband at 1640 cm^{-1} appears, suggesting that K-22 has been covalently grafted onto the surface of $CoFe_2O_4$@3D-Network polymers (Fig. 1C) [42]. Any minor discrepancies between the spectra of the final product and the preceding materials could be due to the addition of Palladium and its interaction with the internal scaffold.

3.1.2 FE-SEM Studies

The FESEM is a useful method that is used to determine the morphology and size distribution of the prepared nanoparticles. FESEM images of the 3D-Network polymers and the $CoFe_2O_4$@3D-Network polymers-K22.Pd catalyst are displayed in Fig. 2. As it is seen, the 3D-Network polymers exhibit a spherical structure with uniformity (Fig. 2a). Furthermore, as shown in the image $CoFe_2O_4$@3D-Network polymers-K22.Pd comparing to the FESEM image of 3D-Network polymers, it was confirmed that some particles were anchored onto the surface of 3D-Network polymers, indicating the presence of $CoFe_2O_4$ nanoparticles and the K22.Pd complex with nano dimensions below 30 nm on the surface (Fig. 2b and c).

3.1.3 TEM Studies

To lend further support to the morphology of the synthesized catalyst, we also include the TEM images in our study. In Fig. 3, the $CoFe_2O_4$ and Pd nanoparticles with spherical morphology are shown as dark spots [43]. In contrast, poly calix[4]resorcinarene might be recognized by transparent colour in the TEM images [44]. This result shows that the magnetic nanoparticles were incorporated in the poly calix[4]resorcinarene successfully and the size of the nanocatalysts is less than 50 nm.

3.1.4 EDX Studies

The EDX (Energy-Dispersive X-ray) analysis, which has confirmed the presence of Co, Si, Fe, N, C, O, and Pd elements, is a strong indication that our catalyst has been synthesized as intended (Fig. 4). Furthermore, the elemental mapping results showing a uniform distribution of these elements throughout the 3D-Network polymers suggest a well-dispersed and integrated system. This homogeneous

Fig. 1 FT-IR spectra of 3D-Network polymers (**A**), $CoFe_2O_4$@3D-Network polymers (**B**), $CoFe_2O_4$@3D-Network polymers-K22 (**C**), $CoFe_2O_4$@3D-Network polymers-K22.Pd (**D**)

Fig. 2 FESEM images of 3D-Network polymers at **a** 200 nm, CoFe$_2$O$_4$@3D-Network polymers-K22.Pd at **b** 200 nm, **c** 10 μ
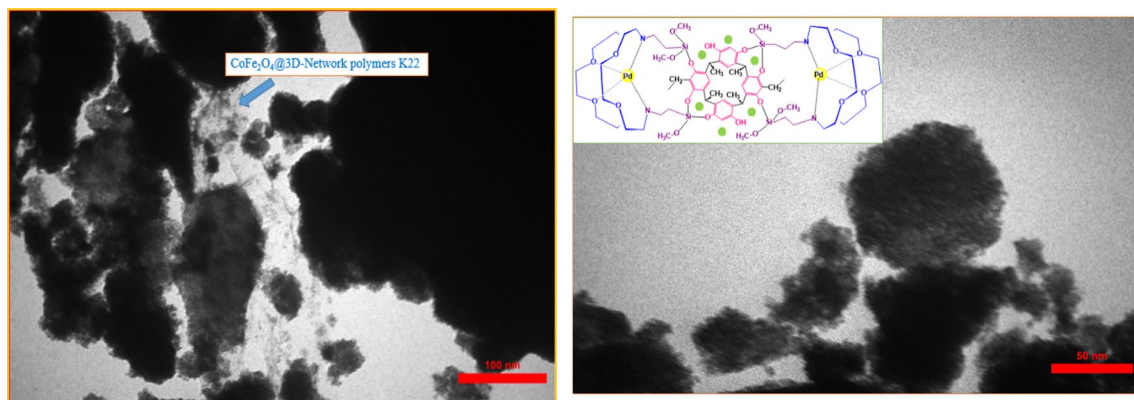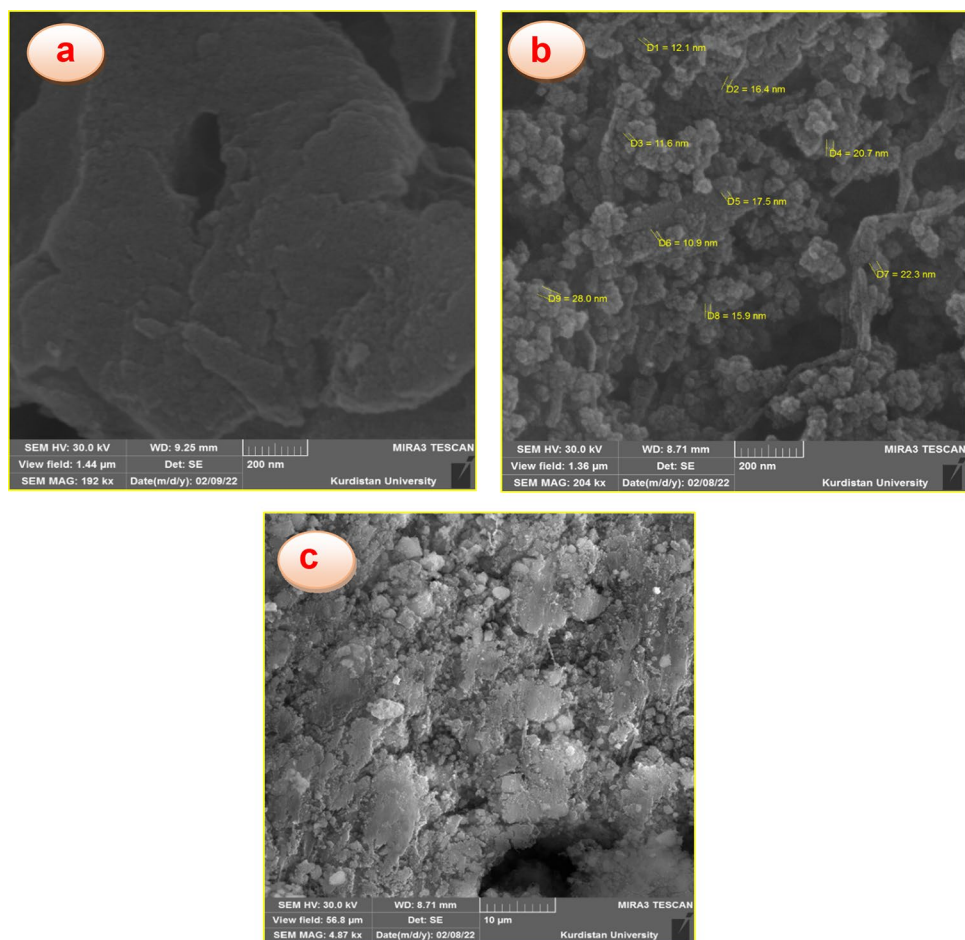

Fig. 3 The TEM image of CoFe$_2$O$_4$@3D-Network polymers-K22.Pd

distribution is often desirable in catalysts, as it ensures a large number of active sites and can lead to better catalytic performance (Fig. 4).

3.1.5 TGA Studies

To evaluate the thermal stability of the prepared catalytic system, thermo-gravimetric analysis (TGA) for 3D-Network polymers (a), CoFe$_2$O$_4$@3D-Network polymers (b) and CoFe$_2$O$_4$@3D-Network polymers-K22.Pd (c) nanostructures were carried out in the temperature range of
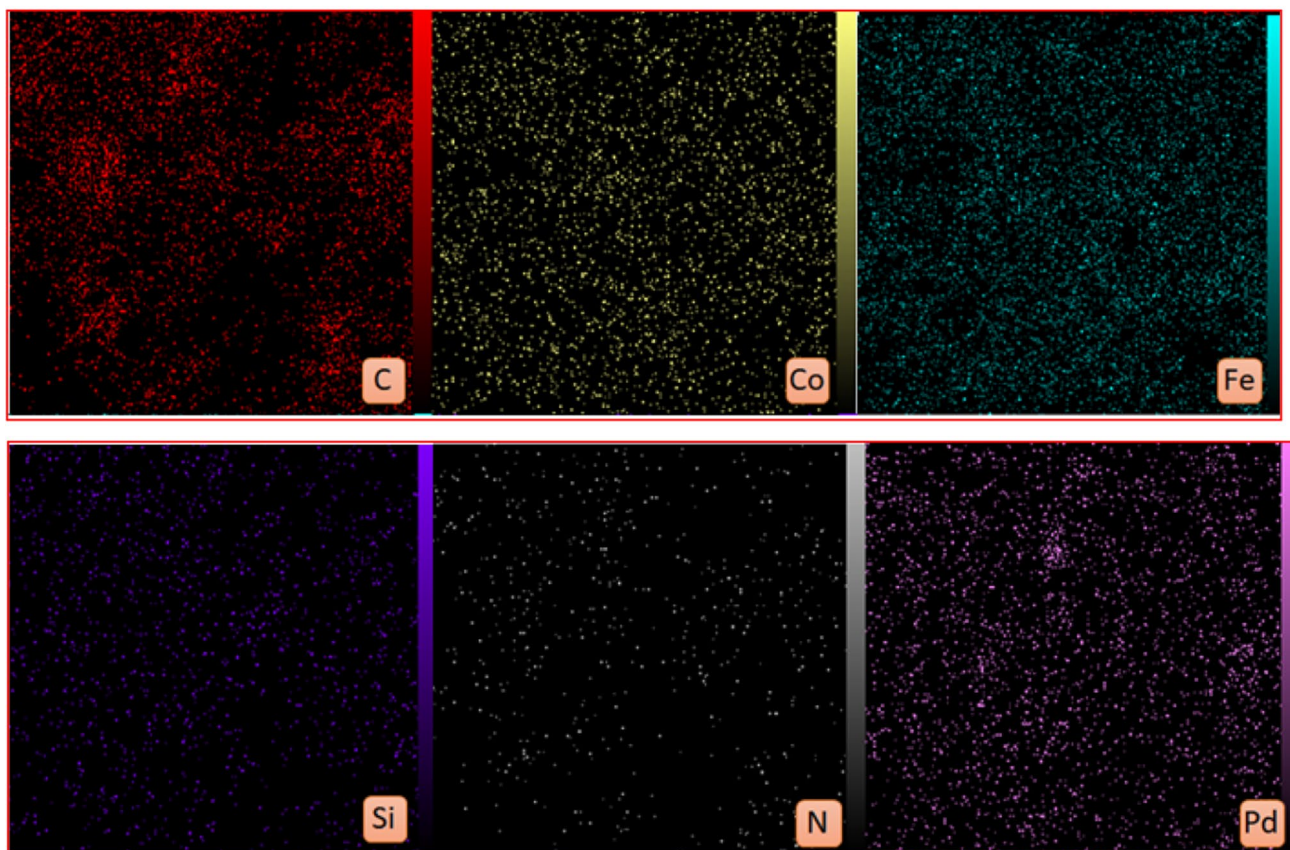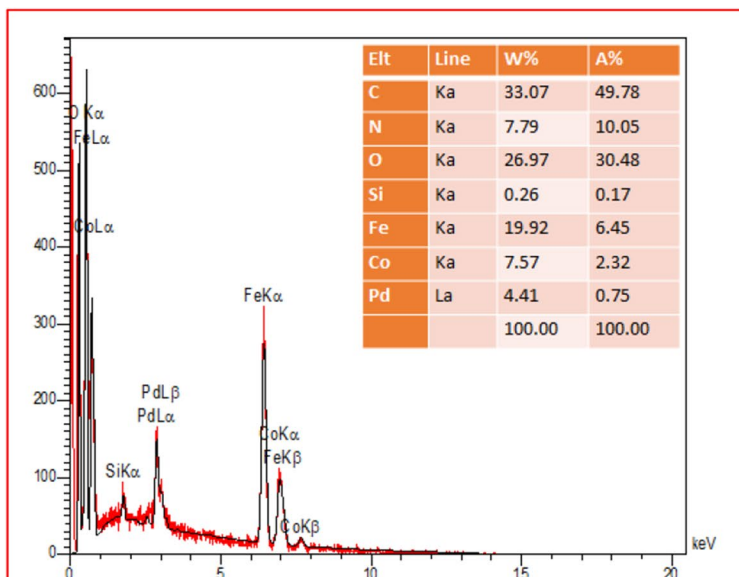
Fig. 4 EDX spectra and X-ray atomic map analysis of $CoFe_2O_4$@3D-Network polymers-K22.Pd

25–850 °C (Fig. 5). The results of the thermal analysis expressed that the thermal stability of 3D-Network polymers and $CoFe_2O_4$@3D-Network polymers are up to nearly 300 °C (Fig. 5a and b).

An initial weight loss (3.2%) between 60 and 150 °C due to the removal of physically adsorbed water during the procedure of the mentioned catalyst occurred. The second weight loss (17.6%) in the temperature range from 180 to 440 °C probably corresponds to the thermal decomposition of the attached groups of 3-(Chloropropyl)-trimethoxysilane and Kryptofix-22. Finally, an essential mass loss of about (23.9%) started from the region of 460 °C can be ascribed
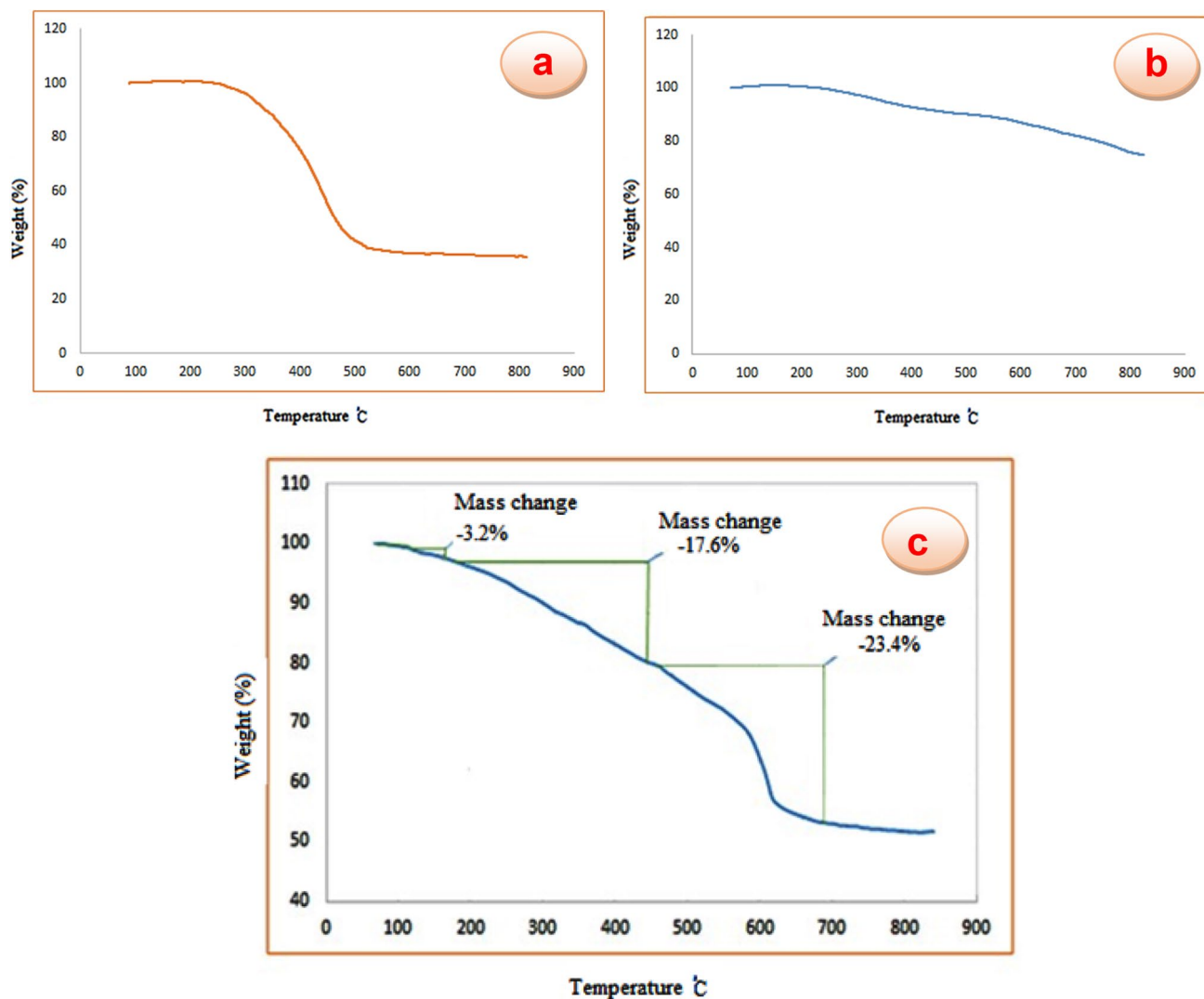
Fig. 5 TGA curves of 3D-Network polymers (**a**), CoFe$_2$O$_4$@3D-Network polymers (**b**) and CoFe$_2$O$_4$@3D-Network polymers-K22.Pd (**c**)

to the decomposition of the anchored polymeric units. This thermal stability profile is favourable in processes where high-temperature catalyst stability is crucial. It suggests a significant level of chemical.

3.1.6 XRD Patterns Studies

X-ray diffraction patterns of the CoFe$_2$O$_4$ (A) and the CoFe$_2$O$_4$@3D-Network polymers-K22.Pd (B) are presented in Fig. 6. The diffraction peaks related to Bragg's reflections from (2 2 0), (3 1 1), (4 0 0), (4 2 2), (3 3 3) and (4 4 0) planes correspond to the standard spinel structure of CoFe$_2$O$_4$ (JCPDS card No. 22-1086). As for the XRD pattern of CoFe$_2$O$_4$@3D-Network polymers-K22.Pd, four new diffraction peaks were observed at 37.52°, 45.92°, 63.57, and 74.26°, confirming the fabrication of Pd particles (marked

as asterisk). Based on the Debye–Scherrer equation, the average size of this CoFe$_2$O$_4$ and CoFe$_2$O$_4$@3D-Network polymers-K22.Pd particles are calculated to be nearly 11 and 24 nm, respectively.

3.1.7 VSM Analysis Studies

Magnetic parameters of CoFe$_2$O$_4$ nanoparticles (A) and CoFe$_2$O$_4$@3D-Network polymers-K22.Pd (B) were determined using a vibrating sample magnetometer (VSM), and the results are shown comparatively in Fig. 7. Considering the results, saturated magnetization values of 61.4 and 14.6 emu g^{-1} are recorded for CoFe$_2$O$_4$ nanoparticles and CoFe$_2$O$_4$@3D-Network polymers-K22.Pd respectively. Compared with CoFe$_2$O$_4$ nanoparticles, a decrease of about 46.8 emu g^{-1} in saturation magnetization of CoFe$_2$O$_4$@3D-Network polymers-K22.Pd can be

Fig. 6 X-ray diffraction (XRD) pattern of $CoFe_2O_4$ (**A**) and $CoFe_2O_4$@3D-Network polymers-K22.Pd (**B**)
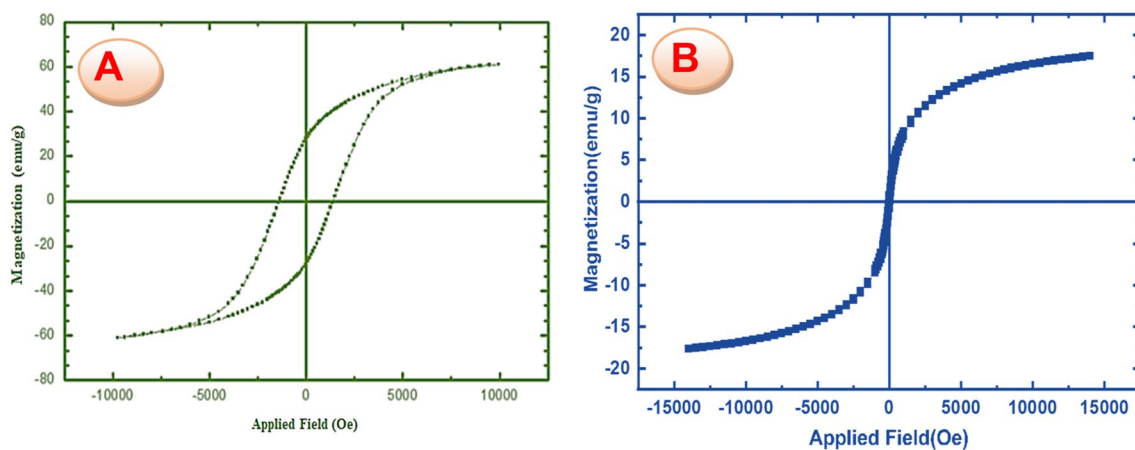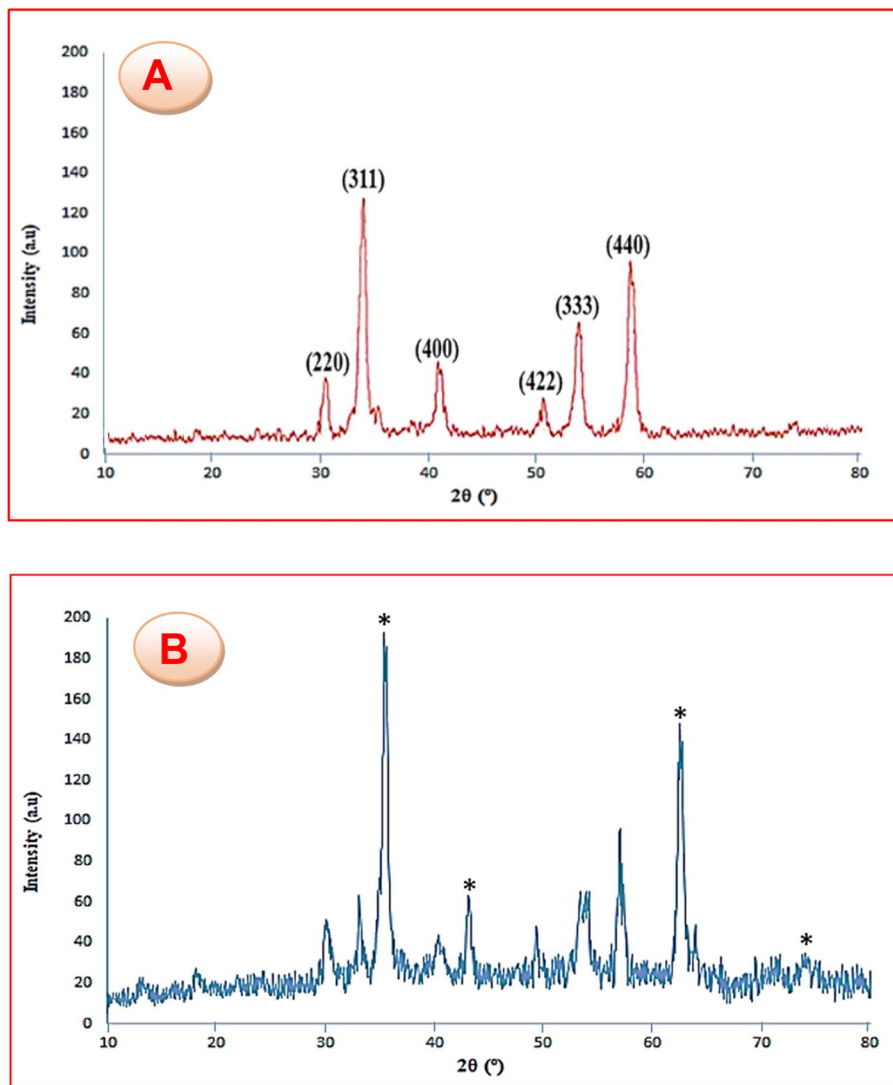

Fig. 7 Magnetization curves of $CoFe_2O_4$ (**A**), $CoFe_2O_4$@3D-Network polymers-K22.Pd (**B**)

attributed to the addition of the non-magnetic components which dilutes the magnetic phase, causing a decrease in magnetization [45,46]. However, even with this reduction in magnetic saturation, the $CoFe_2O_4$@3D-Network polymers-K22.Pd still retains sufficient magnetic properties to allow for easy separation from the reaction solution using an external magnetic field. This is a significant advantage for catalyst recovery and reuse in reactions.

3.1.8 N_2 Adsorption–Desorption Isotherms Studies

Figure 8 the nitrogen adsorption–desorption isotherms and pore size distributions of $CoFe_2O_4$@3D-Network polymers-K22.Pd is illustrated. The materials had type IV isotherms, indicating that the mesostructure remained. According to Brunauer–Emmett–Teller (BET) analysis, the surface area, the pore volume, and the pore size of the catalyst is 17.95 m^2 g^{-1}, 0.2 cm^3 g^{-1}, and 2.78 nm, respectively. Results indicate that immobilizing of the Pd nanoparticles depositing inside the cavities of the K22 and onto the surface of magnetic 3D-Network polymers, may be the reason of reduction the pore volume, pore size, and surface area of the catalysts.

3.2 Catalytic Studies

We characterized the $CoFe_2O_4$@3D-Network polymers-K22.Pd nanocatalyst and then focused on optimizing its catalytic efficiency for nitrobenzene reduction. Our study evaluated the impact of various reaction parameters including temperature, choice of reducing agents, solvent type, and catalyst quantity (Table 1).

Different reducing agents, iPrOH and HCOOH, were compared for the reduction of nitrobenzene, but sodium borohydride ($NaBH_4$) was found to be more effective (Table 2, entries 15–16). Without $NaBH_4$, the reaction didn't occur, and with lower amounts, the yield was minimal (Table 2, entries 10–13). The reaction was ineffective without the catalyst and showed reduced yields with minimal catalyst amounts (Table 2, entry 1). Various solvents were tested, and water (H_2O) proved to be the most suitable. Nonpolar solvents failed to facilitate the reaction (Table 2, entries 2–7). So, the optimized reaction conditions are a 1:1 molar ratio of nitrobenzene to $NaBH_4$, using water as the solvent at room temperature, and using 0.03 g of the $CoFe_2O_4$@3D-Network polymers-K22.Pd nanocatalyst. Under these conditions, the reaction completes in 15 min and affords aniline as the sole product in high yield (Table 2, entry 8). This showcases the effectiveness of the $CoFe_2O_4$@3D-Network polymers-K22.Pd nanocatalyst in reducing nitrobenzene, especially considering the speed and efficiency of the reaction under optimized conditions.

The additional testing of various nitro compounds, both with electron-donating and electron-withdrawing groups, under the previously optimized conditions seems to yield positive results. Good to excellent yields in a short timeframe without any by-product formation point to the efficiency and selectivity of the $CoFe_2O_4$@3D-Network polymers-K22.Pd nanocatalyst in reducing these compounds to arylamines. The lack of selectivity between nitro and aldehyde groups, with both being reduced at a similar rate is noteworthy. It suggests that the catalyst could be useful in scenarios where both functional groups are present without significantly affecting the reaction's outcome (Table 2, entries 5 and 7). Finally, the rapid and efficient reduction of primary aliphatic nitro compounds to their corresponding amines further underscores the catalyst's applicability and efficacy. The broad substrate scope and the impressive reported yields demonstrate the catalyst's potential for the synthesis of arylamines from a diverse range of nitro compounds (Table 2, entry 10).
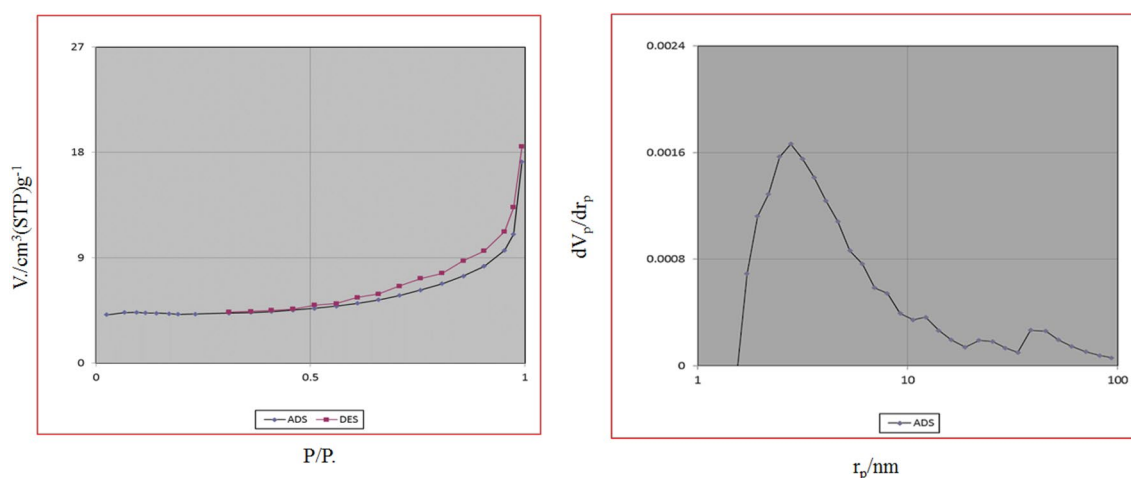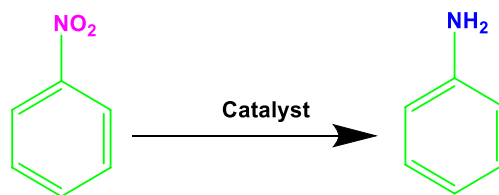

Fig. 8 Nitrogen adsorption–desorption isotherms and BJH pore size distributions of $CoFe_2O_4$@3D-Network polymers-K22.Pd

Table 1 Optimizing the model reaction conditions to reduce nitrobenzene[a] using $CoFe_2O_4$@3D-Network polymers-K22.Pd

Entry	Catalysts amount (mg)	Reducing agent	Solvent	Time (min)	Yield (%)
1	–	$NaBH_4$ (2mmol)	H_2O	100	–
2	30	$NaBH_4$ (1mmol)	n-Hexane	130	–
3	30	$NaBH_4$ (1mmol)	CH_3CN	120	40
4	30	$NaBH_4$ (1mmol)	CH_2Cl_2	100	–
5	30	$NaBH_4$ (1mmol)	Toluene	90	25
6	30	$NaBH_4$ (1mmol)	EtOH	45	77
7	30	$NaBH_4$ (1 mmol)	EtOAc	100	–
8	30	$NaBH_4$ (1mmol)	H_2O	15	98
9	30	$NaBH_4$ (1.25mmol)	H_2O	15	98
10	30	$NaBH_4$ (0.75mmol)	H_2O	40	95
11	30	$NaBH_4$ (0.5mmol)	H_2O	50	90
12	30	$NaBH_4$ (0.25mmol)	H_2O	50	65
13	30	-	H_2O	120	–
14	$CoFe_2O_4$@3D-Network polymers	$NaBH_4$ (1mmol)	H_2O	100	70
15	30	[i]PrOH	_	400	50
16	30	HCOOH	H_2O	30	52

[a]Reaction conditions: nitrobenzene (1 mmol), H_2O (4 mL)

The proposed mechanism for the reduction of nitroarene compounds to aminobenzene derivatives in the presence of $CoFe_2O_4$@3D-Network polymers-K22.Pd nanocatalyst and using sodium borohydride as a hydrogen source is presented in Scheme 2 based on the previously reported mechanism [49].

A plausible mechanism for the catalytic activity of nano $CoFe_2O_4$@3D-Network polymers-K22.Pd is depicted in Scheme 2. The nanocatalyst facilitates the reduction of nitro groups, involving four distinct steps in the nitro reduction process. Initially, hydrogen absorption takes place, followed by adsorption on the metal surfaces. In the third stage, there is an electron transfer through metal surfaces from BH_4^- to aromatic nitro compounds. Subsequently, aromatic amino compounds desorb from the catalyst surface. During this process, B–H bond cleavage occurs on the surface of $CoFe_2O_4$@3D-Network polymers-K22.Pd nanocatalyst [43].

A comparison of the efficiency of the catalytic activity of $CoFe_2O_4$@3D-Network polymers-K22.Pd in the reduction of diverse nitro compounds (Table 3, entries 2–8) with several previously reported methods is presented. Recently, the use of γ-Fe_2O_3/ NPC-600 (Table 3, entry 2), Pd/MIL-101 (Table 3, entry 3), Pt/CoFe-LDH (Table 3, entry 4), UiO-66-d-PANI–AgPd (Table 3, entry 5) and Ni-MoO_3/CN@SBA-15(Table 3, entry 8) as catalyst have been reported for reduction of nitro compounds. These procedures require

Table 2 Reduction of nitro compounds with NaBH$_4$ in the presence of CoFe$_2$O$_4$@3D-Network polymers-K22.Pd nanocatalyst in H$_2$O at room temperature

$$NO_2 \xrightarrow{\text{Catalyst}} NH_2$$
R $\quad$ R

Entry	Nitro Compound	Product	Time (mine)	Yield[a] (%)	Mp (°C) Found/Reported
1	NO$_2$ (benzene)	NH$_2$ (benzene)	15	98	Oil [32]
2	NO$_2$, NH$_2$ (benzene)	NH$_2$, NH$_2$ (benzene)	15	90	105 [47]
3	NO$_2$, OH (benzene)	NH$_2$, OH (benzene)	17	93	190 [35]
4	NO$_2$, NH$_2$ (benzene)	NH$_2$, NH$_2$ (benzene)	15	95	141 [48]
5	NO$_2$, CH$_2$OH (benzene)	NH$_2$, CH$_2$OH (benzene)	12	95	82 [47]

Table 2 (continued)

Entry	Nitro Compound	Product	Time (mine)	Yield[a] (%)	Mp (°C) Found/ Reported
6			20	91	Oil [35]
7			13	92	93 [47]
8			15	93	Oil [35]
9			17	90	181 [48]
10			15	91	Oil [35]

temperature and longer reaction times. In addition, higher reduction group amounts are found when using Starch-crt@Au (Table 3, entry 6) and Pd-porphyrin@polymer (Table 3, entry 7) as catalysts. It demonstrates the catalytic activity of $CoFe_2O_4$@3D-Network polymers-K22.Pd is superior to some previously reported methods in terms of yield, ease of catalyst separation, reaction time, reaction temperature, and the amount of used catalyst.

The activity of $CoFe_2O_4$@3D-Network polymers-K22.Pd synthesized nanocatalysts in the Suzuki coupling reaction was also investigated. In the model reaction, phenylboronic acid is coupled with iodobenzene. Here, the phenylboronic acid acts as the boron component, which will transmetalate with the palladium catalyst to from a palladium-carbon bond. This iodobenzene is the organic halide, and the iodide will be displaced by the palladium complex. The effects of various reaction conditions, including temperature, reducing agents, solvent, and catalyst amount, were studied (Table 4).

Initially, the effect of the different bases such as NaOH, Et_3N, CS_2CO_3, and K_2CO_3 was studied (Table 5, entries
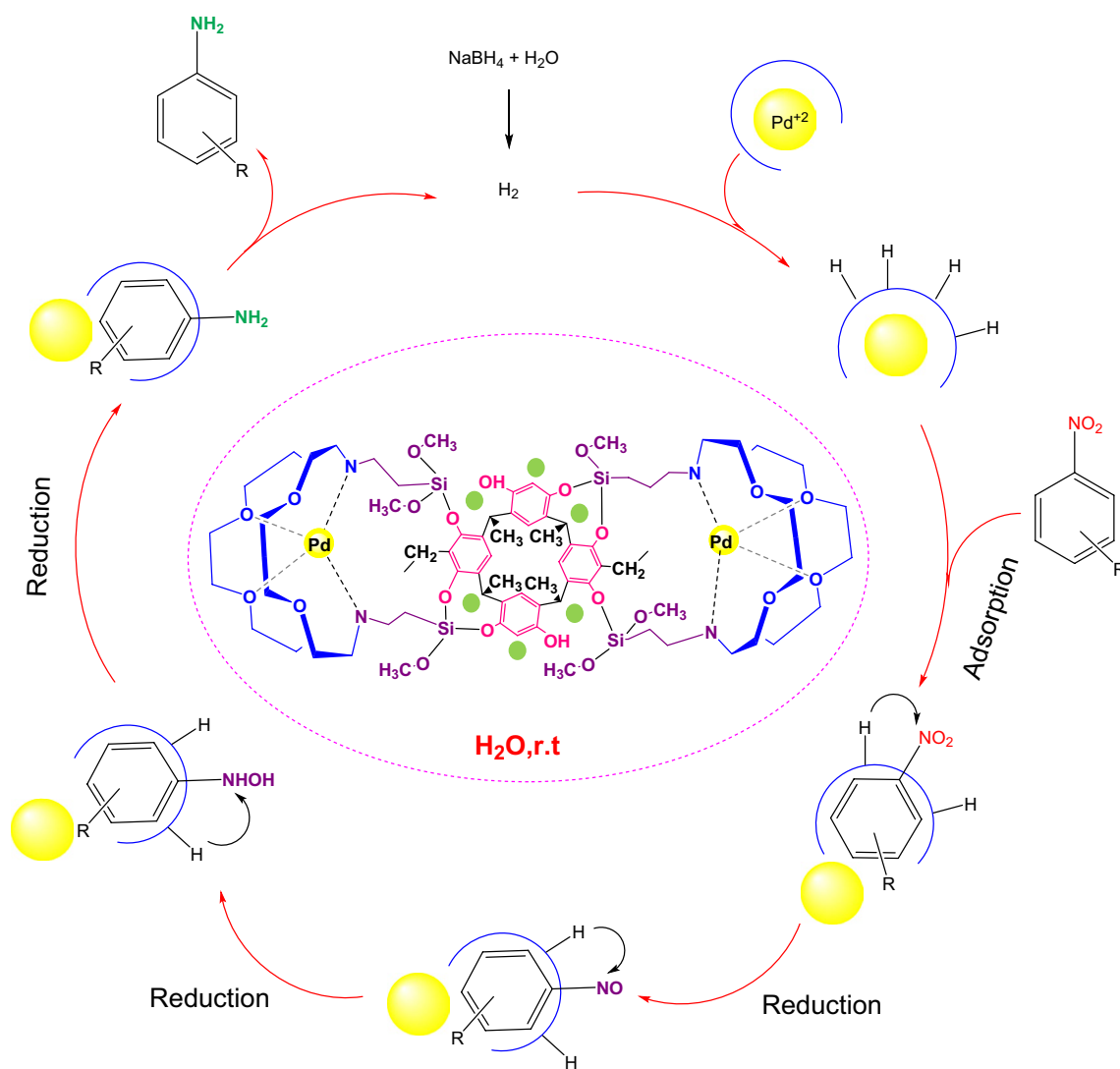
**Scheme 2** A plausible reaction mechanism for reduction of nitrobenzene

Table 3 Comparison of catalytic activity of $CoFe_2O_4$@3D-Network polymers-K22.Pd nanocatalyst with some recently reported procedures

Entry	Catalyst	Time (min)	Reaction Conditions[a]	Yield (%)	References
1	Fe@3D-Network polymers K22.Pd	15	$NaBH_4$, H_2O, r.t	98	This work
2	γ-Fe_2O_3/ NPC-600	60	N_2H_4.H_2O, EtOH, 80 °C	> 99	[50]
3	Pd/MIL-101	6 h	H_2, DMF, 120°C	> 99	[51]
4	Pt/CoFe-LDH	60	$NaBH_4$, isopropanol, 70 °C	97	[52]
5	UiO-66-d-PANI–AgPd	6 h	Formic acid/H_2O/90 °C	99	[53]
6	Starch-crt@Au	4 h	$NaBH_4$, H_2O: EtOH (1:1), r.t (5 mmol)	99	[54]
7	Pd-porphyrin@polymer	10	$NaBH_4$, H_2O, 55 °C (4 mmol)	98	[55]
8	Ni-MoO_3/CN@SBA-15	30	N_2H_4·H_2O, EtOH, 40 °C	99	[56]

[a]All reaction conditions for reduction of nitrobenzene to aniline

Table 4 Optimization experiments of the Suzuki–Miyaura coupling reaction between iodobenzene[a] and phenylboronic acid using CoFe$_2$O$_4$@3D-Network polymers-K22.Pd
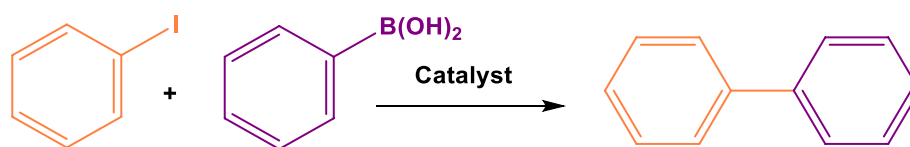

Entry	Catalyst amount (mg)	Base	Condition	Time (min)	Yield (%)
1	–	K$_2$CO$_3$ (2.5 mmol)	H$_2$O /80°C	180	–
2	30	K$_2$CO$_3$ (1.5 mmol)	H$_2$O-EtOH / 80 °C	30	86
3	30	K$_2$CO$_3$ (1.5 mmol)	DMF/100 °C	75	90
4	30	K$_2$CO$_3$ (1.5 mmol)	DMSO/100 °C	105	85
5	30	K$_2$CO$_3$ (1.5 mmol)	EtOH/80 °C	65	82
6	30	K$_2$CO$_3$ (1.5 mmol)	Toluene/100 °C	120	76
7	30	K$_2$CO$_3$ (1.5 mmol)	H$_2$O/ r.t	9	98
8	25	K$_2$CO$_3$ (1.5 mmol)	H$_2$O/ r.t	15	84
9	10	K$_2$CO$_3$ (1.5 mmol)	H$_2$O/ r.t	25	70
10	20	K$_2$CO$_3$ (1.5 mmol)	H$_2$O/ r.t	18	75
11	30	KOH (1.5 mmol)	H$_2$O/ r.t	60	70
12	30	Et$_3$N (1.5 mmol)	H$_2$O/ r.t	70	68
13	30	CS$_2$CO$_3$ (1.5 mmol)	H$_2$O/ r.t	40	90
14	30	NaOH (1.5 mmol)	H$_2$O/ r.t	40	75
15	30	–	H$_2$O/ r.t	140	–

[a]Reaction condition: iodobenzene (1 mmol) and phenylboronic acid (1 mmol) K$_2$CO$_3$ (1.5 mmol), CoFe$_2$O$_4$@3D-Network polymers-K22.Pd (30 mg), and H$_2$O (3 mL)

10–14). The best C–C coupling product was obtained in the presence of K$_2$CO$_3$ as the most effective base with the highest yield of the biphenyl product. Also, Table 5 shows that the reaction did not perform without K$_2$CO$_3$ (Table 5, entry 15). Then, the influence of different solvents such as DMF DMSO, Toluene, H$_2$O, and EtOH on the outcome of the reaction was studied and it was found that H$_2$O is a suitable solvent for this reaction (Table 5, entries 2–7). Eventually, the effect of the catalyst amount on the reaction yield was studied. As shown in Table 5, the use of 30 mg of CoFe$_2$O$_4$@3D- Network polymers-K22.Pd nanocatalyst is sufficient to complete the reaction in 9 min (Table 5, entries 7–10). Meanwhile, without the catalyst, the reaction
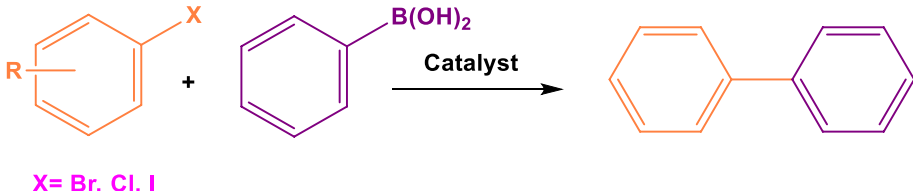
did not proceed at all, even after 180 min (Table 5, entry 1). This result confirms that optimum conditions in the Suzuki coupling reaction as a sole product in high yield was in the presence of K$_2$CO$_3$ and H$_2$O solvent at room temperature in the 30 mg of CoFe$_2$O$_4$@3D-Network polymers-K22.Pd nanocatalyst. After obtaining the appropriate optimal conditions, we employed diverse aryl halide compound derivatives for the Suzuki reaction.
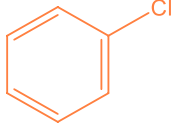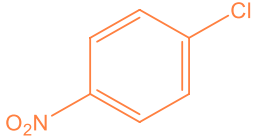
In our further studies using various aryl halide compounds for the Suzuki reaction, we found that both electron-donating and electron-withdrawing groups yield moderate to excellent products in a short time, without producing any byproducts. However, the reactions with aryl chlorides were

Table 5 Suzuki C–C cross-coupling reaction[a] in the presence of CoFe$_2$O$_4$@3D-Network polymers-K22.Pd nanocatalyst

X= Br, Cl, I
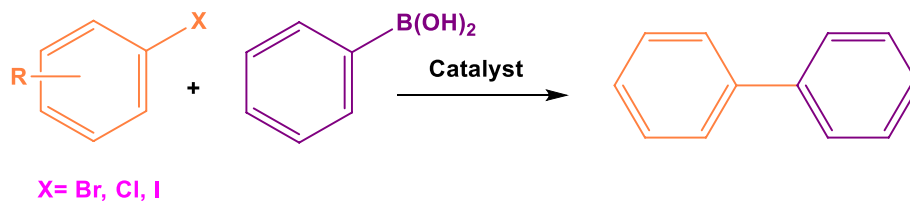
Entry	Aryl halide	Product	Time (min)	Yield (%)	Mp (°C) Found/ Reported
1			20	99	64–65 [57]
2			60	91	82–83 [58]
3			70	95	86–90 [58]
4			63	98	86–87 [[59]]
5			78	97	75–79 [58]
6			9	99	63–64 [58]
7			25	97	83–84 [60]
8			15	96	64–65 [60]

Table 5 (continued)

X= Br, Cl, I

| Entry	Aryl halide	Product	Time (min)	Yield (%)	Mp (°C) Found/Reported
9			40	99	68–69 [61]
10			75	91	112–113 [62]

[a]Reaction conditions: phenylboronic acid (1 mmol), various aryl halides (1 mmol), K_2CO_3 (1.5 mmol), solvent (3 mL), and $CoFe_2O_4$@3D-Network polymers-K22.Pd (30 mg) at room temperature

slower compared to their iodide or bromide counterparts due to their lower reactivity and leaving capacity, resulting in moderate yields (Table 5).

The proposed mechanism for Suzuki cross-coupling in the presence of $CoFe_2O_4$@3D-Network polymers-K22.Pd nanocatalyst involves three fundamental steps: The first step is the oxidative addition of the aryl halide to the $CoFe_2O_4$@3D-Network polymers-K22.Pd nanocatalyst, forming an intermediate (1), which is a $CoFe_2O_4$@3D-Network polymers-K22.Pd (II) species. This is followed by the transmetalation step, where the phenylboron compound reacts with intermediate 1 to form intermediate (2). Finally, in the reductive elimination step, the desired product is formed, and the $CoFe_2O_4$@3D-Network polymers-K22.Pd catalyst is regenerated, and ready to participate in another reaction cycle (Scheme 3).

3.3 Comparison of the Catalyst

Our comparative study suggests that the $CoFe_2O_4$@3D-Network polymers-K22.Pd nanocatalyst shows improved performance over several previously reported catalysts, in the context of the Suzuki–Miyaura cross-coupling reaction (Table 6). Important factors such as ease of catalyst separation, yield, reaction time, and reaction temperature demonstrate its superiority. This catalyst appears to offer an efficient and environmentally friendly solution for carrying out this important transformation.
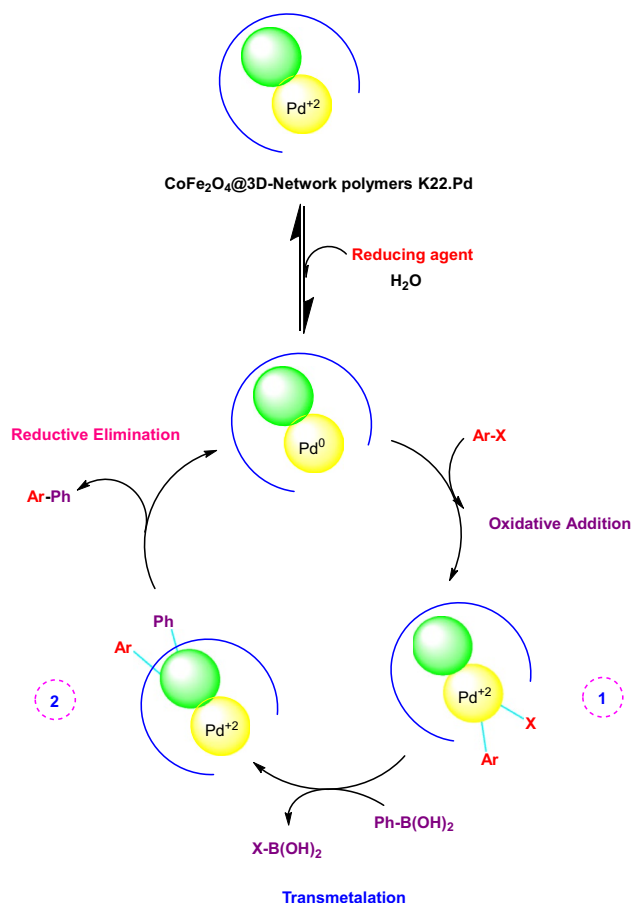
Scheme 3 The plausible reaction mechanism synthesis for the Suzuki coupling reaction

Table 6 Comparison of the catalytic activity of CoFe$_2$O$_4$@3D-Network polymers-K22.Pd nanocatalyst in the Suzuki coupling reaction of iodobenzene with some recently reported procedures

Entry	Catalyst	X	Time (min)	Reaction Conditions	Yield (%)	References
1	CoFe$_2$O$_4$@3D-Network polymers K22.Pd	I	9	K$_2$CO$_3$, H$_2$O, r.t	98	This work
2	Pd/AlO(OH) NPs	Br	2 h	N$_2$H$_4$. H$_2$O-IPA, 80 °C	98	[63]
3	PSCOP-Pd(II)	Br	90	K$_2$CO$_3$, toluene, 110°C	> 99	[64]
4	Pd/SBA-15	Br	90	K$_2$CO$_3$, Ethanol, 60 °C	99	[65]
5	Pd@PS-Met	Br	6 h	K$_2$CO$_3$/H$_2$O/80 °C	90	[66]
6	Pd(OAc)$_2$	Br-I	16 h	NaOH, H$_2$O	100	[67]
7	PdAu/Fe$_3$O$_4$	Br	9 h	K$_2$CO$_3$, DMF, 90 °C	98	[68]
8	magnetic Z-Y − Pd − NF	Br	2 h	K$_2$CO$_3$, H$_2$O/EtOH, 80 °C	83	[69]

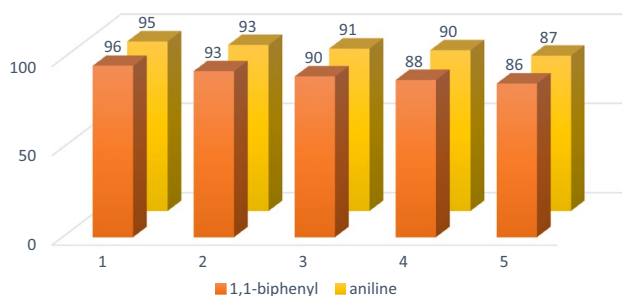**Fig. 9** Recyclability of CoFe$_2$O$_4$@3D-Network polymers-K22.Pd in the synthesis of 1,1-biphenyl and aniline

4 Recycling of CoFe$_2$O$_4$@3D-Network Polymers-K22.Pd Catalyst

Encouraged by the high catalytic activity of the nanocatalyst, the recyclability of CoFe$_2$O$_4$@3D-Network polymers-K22.Pd was investigated. The recyclability was studied for the reduction of nitrobenzene with NaBH$_4$ and also the Suzuki–Miyaura reaction between iodobenzene and phenylboronic acid as model reactions. As described in the experimental section, the magnetically recovered CoFe$_2$O$_4$@3D-Network polymers-K22.Pd was washed, dried, and applied for the next run of the reaction. As shown in Fig. 9, the catalyst can be recycled for five runs without any considerable loss of catalytic activity.

In the following, the structure of recycled CoFe$_2$O$_4$@3D-Network polymers-K22.Pd was studied by FT-IR, XRD, EDX, and FE-SEM analyses Fig. 10. As shown, the FT-IR spectrum of the catalyst is almost similar to that of the fresh CoFe$_2$O$_4$@3D-Network polymers-K22.Pd. However, the change in the intensities of some bands is observed. FE-SEM, EDX, and XRD analyses of this catalyst showed that CoFe$_2$O$_4$@3D-Network polymers-K22.Pd maintained its chemical structure after the longevity tests.

The recovered catalyst was reused in five cycles without considerable loss of its catalytic activity. FT-IR, XRD, EDX and FE-SEM analyses were carried out and the results are displayed below (Fig. 10). These analyses showed that the CoFe$_2$O$_4$@3D-Network polymers-K22.Pd catalyst maintained its chemical structure during the catalytic process.

5 Conclusions

In the present work, we successfully reported a novel, recoverable, and thermally stable heterogeneous catalytic system, CoFe$_2$O$_4$@3D-Network polymers-K22.Pd, achieved by anchoring Pd on the Kryptofix-22 modified magnetic 3D-Network polymers. To evaluate its applicability in organic reactions, this porous organic polymer-based catalyst was utilized in the synthesis of Suzuki reactions and reduction of nitro compounds derivatives. The introduced catalyst can be easily separated from the reaction mixture using a magnetic force and reused in 5 repetitions without
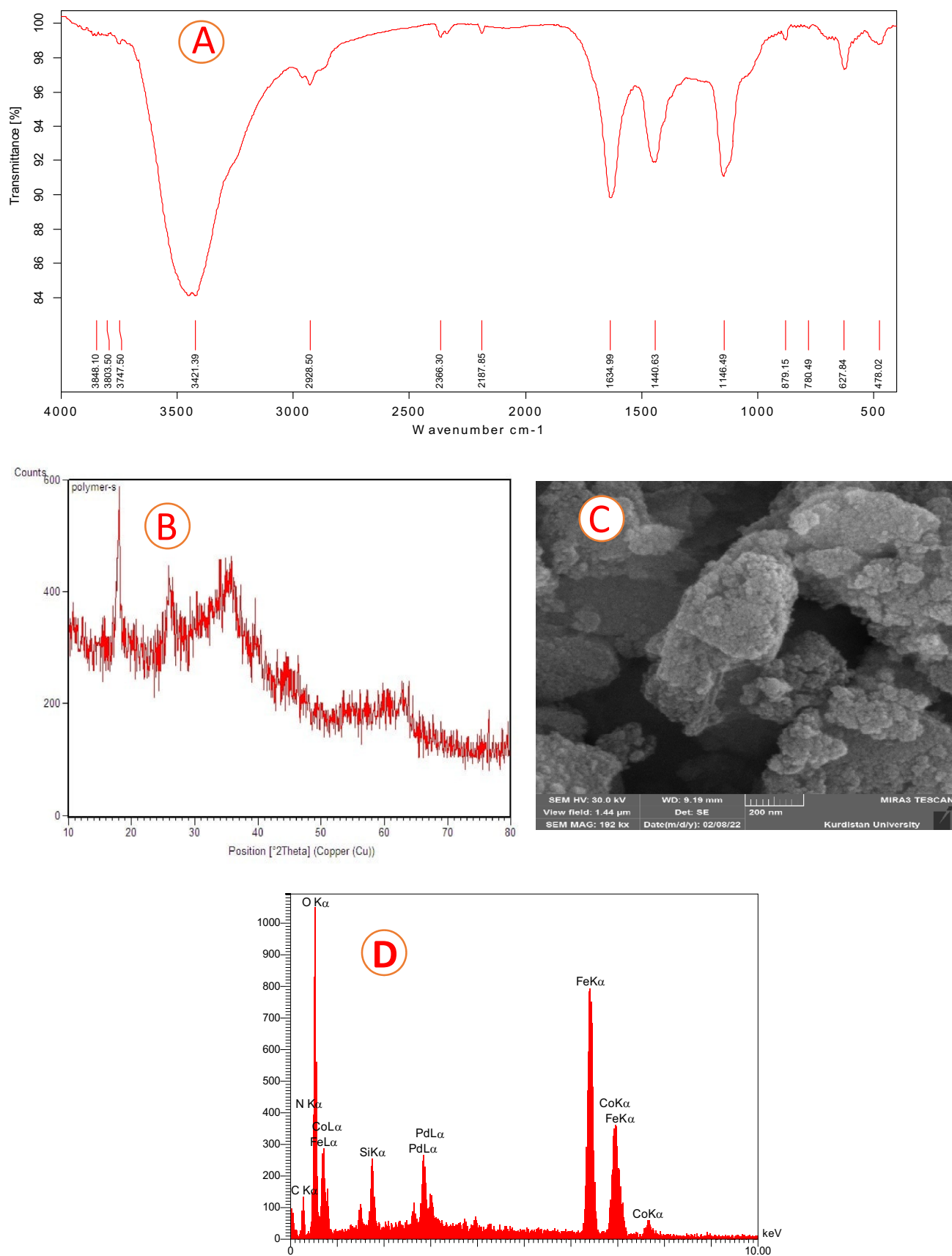
Fig. 10 FT-IR (**A**), XRD (**B**) SEM (**C**), and EDX analyses (**D**), of the reused catalyst after five run

significant activity loss. The green protocol is highly desirable in terms of activity, high yields, stability, and the easy separation of the catalyst. We expect this new and practical protocol to be widely used in drug development and academia.

Data Availability No datasets were generated or analysed during the current study.

Declarations

Competing interests The authors declare no competing interests.

References

1. A. Adam, D. Mertz, Nanomaterial. (2023). https://doi.org/10.3390/nano13081342
2. Y. Xiao, J. Du, J. Mater. Chem. B. **8**, 354–367 (2020)
3. M. Bustamante-Torres, D. Romero-Fierro, B. Arcentales-Vera, S. Pardo, E. Bucio, Polymers (2021). https://doi.org/10.3390/polym13172998
4. L.R. Shultz, K. Preradovic, S. Ghimire, H.M. Hadley, S. Xie, V. Kashyap, M.J. Beazley, K.E. Crawford, F. Liu, K. Mukhopadhyay, T. Jurca, Catal. Sci. Technol. **12**, 3804–3816 (2022)
5. L. Van Emelen, V. Lemmens, C. Marquez, S. Van Minnebruggen, O.A. Usoltsev, A.L. Bugaev, K. Janssens, K.Y. Cheung, N. Van Velthoven, D. De Vos, ACS Appl Mater. Interface. **14**, 51867–51880 (2022)
6. M. Nandeshwar, S. Mandal, S. Kuppuswamy, G. Prabusankar, Chem Asian J. (2022). https://doi.org/10.1002/asia.202201138
7. A. Giri, A. Patra, Chem. Rec. (2022). https://doi.org/10.1002/tcr.202200071
8. Z. Wang, Y. Liu, Y. Zhao, Q. Zhang, Y. Sun, B. Yang, J. Bu, Z. Chun, RSC Adv. **12**, 16486–16490 (2022)
9. S. Daliran, A.R. Oveisi, Y. Peng, A. López-Magano, M. Khajeh, R. Mas-Ballesté, J.V. Alemán, R. Luque, H. García, Chem. Soc. Rev. **51**, 7810–7882 (2022)
10. Q. Sun, B. Aguila, Y. Song, S. Ma, Acc. Chem. Res. **53**, 812–821 (2020)
11. B. Li, K.M. Kwok, H.C. Zeng, A.C.S. Appl, Mater. Interface. **13**, 20524–20538 (2021)
12. C.T. Buru, O.K. Farha, A.C.S. Appl, Mater. Interfaces. **12**, 5345–5360 (2020)
13. W.Y. Pei, G. Xu, J. Yang, H. Wu, B. Chen, W. Zhou, J. Fang, J. Am. Chem. Soc. **139**, 7648–7656 (2017)
14. R.R. Kashapov, Y. Razuvayeva, A.Y. Ziganshina, R.K. Mukhitova, A.S. Sapunova, A.D. Voloshina, V.V. Syakaev, S.K. Latypov, I.R. Nizameev, I.M.K. Kadirov, L.Y. Zakharova, Molecules (2019). https://doi.org/10.3390/molecules24101939
15. D. Luo, M. Li, Q. Ma, G. Wen, H. Dou, B. Ren, Y. Liu, X. Wang, L. Shui, Z. Chen, Chem. Soc. Rev. **51**, 2917–2938 (2022)
16. S. Guo, T.M. Swager, J. Am. Chem. Soc. **143**, 11828–11835 (2021)
17. P. Lhoták, Org. Biomol. Chem. **20**, 7377–7390 (2022)
18. A.G. Coman, C. Stavarache, A. Păun, C.C. Popescu, N.D. Hădade, P. Ionita, M. Matache, RSC Adv. **9**, 6078–6083 (2019)
19. S.A. Ansari, A. Bhattacharyya, P.K. Mohapatra, R.J. Egberink, J. Huskens, W. Verboom, RSC Adv. **9**, 31928–31935 (2019)
20. R. Mozafari, F. Heidarizadeh, F. Nikpour, Mater. Sci. Eng. C. (2019). https://doi.org/10.1016/j.msec.2019.110109
21. Z. Zhao, H. Tian, M. Zhang, Y. Yang, H. Zhang, Environ. Sci. Pollut. Res. **25**, 34550–34558 (2018)
22. Z. Tian, Y. Wang, Y. Li, Y. Ge, Q. Zhang, L. Chen, Science. (2022). https://doi.org/10.1016/j.isci.2022.104557
23. E. Sikora, D. Koncz-Horváth, G. Muránszky, F. Kristály, B. Fiser, B. Viskolcz, L. Vanyorek, Int. J. Mol. Sci. (2021). https://doi.org/10.3390/ijms222111846
24. B. Li, K.M. Kwok, H.C. Zeng, A.C.S. Appl, Mater. Interfaces. **13**, 20524–20538 (2021)
25. M. Enneiymy, P. Fioux, C.L. Drian, C.M. Ghimbeu, J. Becht, RSC Adv. **10**, 36741–36750 (2020)
26. A. Assefa, F. Ren, J. Liu, W. Zheng, Q. Song, W. Jia, J. Bao, Y. Li, RSC Adv. **11**, 33692–33702 (2021)
27. S. Choi, S. Ilyas, G. Hwang, H. Kim, J. Environ. Manage. (2021). https://doi.org/10.1016/j.jenvman.2021.112748
28. A. Lin, A. Ibrahim, P. Arab, H.M. El-Kaderi, M.S. El-Shall, A.C.S. Appl, Mate. Interfaces. **9**, 17961–17968 (2017)
29. T. Seo, T. Ishiyama, K. Kubota, H. Ito, Chem. Sci. **10**, 8202–8210 (2019)
30. E. Tessema, V. Elakkat, C. Chiu, Z. Tsai, K.L. Chan, C. Shen, H. Su, N. Lu, Molecules (2021). https://doi.org/10.3390/molecules26051414
31. J. Li, X. Zhang, Y. Yao, Y. Gao, W. Yang, W. Zhao, J. Org. Chem. **87**, 6951–6959 (2022)
32. B. Zheng, J. Xu, J. Song, H. Wu, X. Mei, K. Zhang, W. Han, W. Wu, M. He, B. Han, Chem. Sci. **13**, 9047–9055 (2022)
33. N. Zengin, H. Göksu, F. Sen, Chemosphere. (2021). https://doi.org/10.1016/j.chemosphere.2021.130887
34. A. Kumar, P. Sharma, N. Sharma, Y. Kumar, D. Mahajan, RSC Adv. **11**, 25777–25787 (2021)
35. M. Ghadermazi, S. Moradi, R. Mozafari, RSC Adv. **10**, 33389–33400 (2020)
36. A.M. Asl, B. Karami, Z. Karimi, RSC Adv. **13**, 13374–13383 (2023)
37. X. Huang, W. Zhou, D. Deng, B. Liu, K. Jiang, Materials (2021). https://doi.org/10.3390/ma14247546
38. A. Mouradzadegun, A.R. Kiasat, P.K. Fard, Catal. Commun. **29**, 1–5 (2012)
39. A. Mouradzadegun, M.A. Mostafavi, M.R. Ganjali, J. Inclusion Phenom. Macrocyclic Chem. **91**, 25–36 (2018)
40. R. Tabit, O. Amadine, Y. Essamlali, K. Dânoun, A. Rhihil, M. Zahouily, RSC Adv. **8**, 1351–1360 (2020)
41. M. Ariannezhad, D. Habibi, S. Heydari, Polyhedron **160**, 170–179 (2019)
42. R. Mozafari, M. Ghadermazi, RSC Adv. **10**, 15052–15064 (2020)
43. H. Veisi, A. Rostami, M. Shirinbayan, Appl. Organomet. Chem. (2017). https://doi.org/10.1002/aoc.3609
44. A. Mouradzadegun, M.A. Mostafavi, Polym. Eng. Sci. **58**, 1362–1370 (2018)
45. M. Moradian, A.R. Faraji, A. Davood, Int. J. Biol. Macromol. (2024). https://doi.org/10.1016/j.ijbiomac.2023.127863
46. A. Johan, D. Setiabudidaya, F.S. Arsyad, W.A. Adi, Mater. Chem. Phys. (2023). https://doi.org/10.1016/j.matchemphys.2022.127086
47. S. Sorkhabi, M. Ghadermazi, R. Mozafari, ChemistrySelect **6**, 1–8 (2021)

48. B. Zeynizadeh, F. Sepehraddin, J. Iran. Chem. Soc. **14**, 2649–2657 (2017)
49. X. Han, X. Chen, Y. Zou, S. Zhang, Appl. Catal. B. (2020). https://doi.org/10.1016/j.apcatb.2019.118451
50. V. Babel, B.L. Hiran, Catal. Lett. **10**, 1865–1869 (2020)
51. M. Gholinejad, N. Dasvarz, M. Shojafar, J.M. Sansano, Inorg. Chim. Acta. (2019). https://doi.org/10.1007/s10847-020-01021-x
52. S. Hamid, A. Mouradzadegun, J. Inclusion Phenom. Macrocyclic Chem. **98**, 213–221 (2020)
53. H. Huang, X. Wang, L. Xu, C. Chen, X. Zou, W. Ding, X. Lu, Green Chem. **19**, 809–815 (2017)
54. H. Göksu, N. Zengin, A. Karaosman, F. Sen, Curr. Organocatal. **5**, 34–41 (2018)
55. B.X. Valderrama-García, E. Rufino-Felipe, H. Valdés, S. Hernández-Ortega, B.A. Aguilar-Castillo, D. Morales-Morales, Inorg. Chim. Acta. (2020). https://doi.org/10.1007/s11051-018-4325-0
56. F. Ulusal, E. Erünal, B. Güzel, J. Nanopart. Res. (2018). https://doi.org/10.1007/s11051-018-4325-0
57. M. Nikoorazm, A. Ghorbani-Choghamarani, N. Noori, B. Tahmasbi, Appl. Organometal. Chem. **30**, 843–851 (2016)
58. T. Tamoradi, M. Ghadermazi, Ghorbani-Choghamarani A. Journal of Porous Materials. **26**, 121–131 (2019)
59. L. Bai, J.X. Wang, Adv. Synth. Catal. **350**, 315–320 (2007)
60. P. Zhao, H. Yin, H. Gao, C. Xi, J. Org. Chem. **78**, 5001–5006 (2013)
61. A. Ghorbani-Choghamarani, B. Tahmasbi, P. Moradi, Appl. Organometal. Chem. **30**, 422–430 (2016)
62. Y.Y. Peng, J. Liu, X. Lei, Z. Yin, Green Chem. **12**, 1072–1075 (2010)
63. M.M. Ayad, W.A. Amer, M.G. Kotp, Mol. Catal. **439**, 72–80 (2017)
64. J. Lv, Z. Liu, Z. Dong, Mol. Catal. (2020). https://doi.org/10.1016/j.mcat.2020.111249
65. X. Chen, K. Shen, D. Ding, J. Chen, T. Fan, R. Wu, Y. Li, ACS Catal. **8**, 10641–10648 (2018)
66. H. Veisi, S.A. Mirshokraie, H. Ahmadian, Int. J. Biol. Macromol. **108**, 419–425 (2018)
67. M. Blanco, D. Mosconi, C. Tubaro, A. Biffis, D. Badocco, P. Pastore, M. Otyepka, A. Bakandritsos, Z. Liu, W. Ren, S. Agnoli, G. Granozzi, Green Chem. **21**, 5238–5247 (2019)
68. X. Chen, D. Qian, G. Xu, H. Xu, J. Dai, Y. Du, Colloids Surf. A **573**, 67–72 (2019)
69. M. Dehghani, A. Tadjarodi, S. Chamani, ACS Omega **4**, 10640–10648 (2019)